Supercontinuum pulse shaping in the few-cycle regime

Franz Hagemann, Oliver Gause, Ludger Wöste, and Torsten Siebert[*]

Institut für Experimentalphysik, Freie Universität Berlin, Arnimallee 14, 14195 Berlin

[*]*torsten.siebert@physik.fu-berlin.de*

Abstract: The synthesis of nearly arbitrary supercontinuum pulse forms is demonstrated with sub-pulse structures that maintain a temporal resolution in the few-cycle regime. Spectral broadening of the 35 fs input pulses to supercontinuum bandwidths is attained in a controlled two-stage sequential filamentation in air at atmospheric pressure, facilitating a homogeneous power density over the full spectral envelope in the visible to near infrared spectral range. Only standard optics and a liquid crystal spatial light modulator (LC-SLM) are employed for achieving pulse compression to the sub 5 fs regime with pulse energies of up to 60 μJ and a peak power of 12 GW. This constitutes the starting point for further pulse form synthesis via phase modulation within the sampling limit of the pulse shaper. Transient grating frequency-resolved optical gating (TG-FROG) allows for the characterization of pulse forms that extend over several hundred femtoseconds with few-cycle substructures.

© 2013 Optical Society of America

References and links

1. F. Silva, D. R. Austin, A. Thai, M. Baudisch, M. Hemmer, D. Faccio, A. Couairon, and J. Biegert, "Multi-octave supercontinuum generation from mid-infrared filamentation in a bulk crystal," Nat. Commun. **3**, 807 (2012).
2. E. Goulielmakis, V. S. Yakovlev, A. L. Cavalieri, M. Uiberacker, V. Pervak, A. Apolonski, R. Kienberger, U. Kleineberg, and F. K. D, "Attosecond control and measurement: Lightwave electronics," Science **317**, 769–775 (2007).
3. E. Granados, L.-J. Chen, C.-J. Lai, K.-H. Hong, and F. X. Kaertner, "Wavelength scaling of optimal hollow-core fiber compressors in the single-cycle limit," Opt. Express **20**, 9099–9108 (2012).
4. D. Adolph, A. M. Sayler, T. Rathje, K. Ruehle, and G. G. Paulus, "Improved carrier-envelope phase locking of intense few-cycle laser pulses using above-threshold ionization," Opt. Lett. **36**, 3639–3641 (2011).
5. A. Zheltikov, "Nanoscale nonlinear optics in photonic-crystal fibres," J. Opt. A: Pure Appl. Opt. **8**, S47–S72 (2006).
6. E. E. Serebryannikov, E. Goulielmakis, and A. M. Zheltikov, "Generation of supercontinuum compressible to single-cycle pulse widths in an ionizing gas," New J. Phys. **10**, 093001 (2008).
7. L. Berge, S. Skupin, R. Nuter, J. Kasparian, and J.-P. Wolf, "Ultrashort filaments of light in weakly ionized, optically transparent media," Rep. Prog. Phys. **70**, 1633–1713 (2007).
8. J. Bethge, C. Bree, H. Redlin, G. Stibenz, P. Staudt, G. Steinmeyer, A. Demircan, and S. Duesterer, "Self-compression of 120 fs pulses in a white-light filament," J. Opt. **13**, 055203 (2011).
9. L. Berge, S. Skupin, and G. Steinmeyer, "Temporal Self-Restoration of Compressed Optical Filaments," Phys. Rev. Lett. **101**, 213901 (2008).
10. C. Hauri, W. Kornelis, F. Helbing, A. Heinrich, A. Couairon, A. Mysyrowicz, J. Biegert, and U. Keller, "Generation of intense, carrier-envelope phase-locked few-cycle laser pulses through filamentation," Appl. Phys. B **79**, 673–677 (2004).
11. A. Couairon, M. Franco, A. Mysyrowicz, J. Biegert, and U. Keller, "Pulse self-compression to the single-cycle limit by filamentation in a gas with a pressure gradient," Opt. Lett. **30**, 2657–2659 (2005).

12. A. Guandalini, P. Eckle, M. Anscombe, P. Schlup, J. Biegert, and U. Keller, "5.1 fs pulses generated by filamentation and carrier envelope phase stability analysis," J. Phys. B **39**, 257–264 (2006).

13. G. Méjean, J. Kasparian, J. Yu, S. Frey, E. Salmon, J. P. Wolf, L. Bergé, and S. Skupin, "UV-supercontinuum generated by femtosecond pulse filamentation in air: Meter-range experiments versus nummerical simulations," Appl. Phys. B **82**, 341–345 (2006).

14. P. Béjot, J. Kasparian, and J. Wolf, "Dual-color co-filamentation in argon," Opt. Express **16**, 14115–14127 (2008).

15. P. Béjot, J. Kasparian, and J.-P. Wolf, "Cross compression of light bullets by two-color cofilamentation," Phys. Rev. A **78**, 043804 (2008).

16. N. Akoezbek, S. A. Trushin, A. Baltuska, W. Fuss, E. Goulielmakis, K. Kosma, F. Krausz, S. Panja, M. Uiber-acker, W. E. Schmid, A. Becker, M. Scalora, and M. Bloemer, "Extending the supercontinuum spectrum down to 200 nm with few-cycle pulses," New J. Phys. **8**, 177 (2006).

17. A. Rondi, J. Extermann, L. Bonacina, S. Weber, and J. P. Wolf, "Characterization of a MEMS-based pulse-shaping device in the deep ultraviolet," Appl. Phys. B **96**, 757–761 (2009).

18. S. Demmler, J. Rothhardt, A. M. Heidt, A. Hartung, E. G. Rohwer, H. Bartelt, J. Limpert, and A. Tuennermann, "Generation of high quality, 1.3 cycle pulses by active phase control of an octave spanning supercontinuum," Opt. Express **19**, 20151–20158 (2011).

19. M. Yamashita, K. Yamane, and R. Morita, "Quasi-automatic phase-control technique for chirp compensation of pulses with over-one-octave bandwidth-generation of few- to mono-cycle optical pulses," IEEE J. Sel. Top. Quantum Electron. **12**, 213–222 (2006).

20. B. Xu, Y. Coello, V. V. Lozovoy, D. A. Harris, and M. Dantus, "Pulse shaping of octave spanning femtosecond laser pulses," Opt. Express **14**, 10939–10944 (2006).

21. K. Yamane, Z. Zhang, K. Oka, R. Morita, M. Yamashita, and A. Suguro, "Optical pulse compression to 3.4 fs in the monocycle region by feedback phase compensation," Opt. Lett. **28**, 2258–2260 (2003).

22. B. Schenkel, J. Biegert, U. Keller, C. Vozzi, M. Nisoli, G. Sansone, S. Stagira, S. De Silvestri, and O. Svelto, "Generation of 3.8-fs pulses from adaptive compression of a cascaded hollow fiber supercontinuum," Opt. Lett. **28**, 1987–1989 (2003).

23. A. Prakelt, M. Wollenhaupt, A. Assion, C. Horn, C. Sarpe-Tudoran, M. Winter, and T. Baumert, "Compact, robust, and flexible setup for femtosecond pulse shaping," Rev. Sci. Instr. **74**, 4950–4953 (2003).

24. R. Morita, M. Hirasawa, N. Karasawa, S. Kusaka, N. Nakagawa, K. Yamane, L. Li, A. Suguro, and M. Yamashita, "Sub-5 fs optical pulse characterization," Meas. Sci. Technol. **13**, 1710–1720 (2002).

25. J. Köhler, M. Wollenhaupt, T. Bayer, C. Sarpe, and T. Baumert, "Zeptosecond precision pulse shaping," Opt. Express **19**, 11638–11653 (2011).

26. A. Poppe, R. Holzwarth, A. Apolonski, G. Tempea, C. Spielmann, T. Hansch, and F. Krausz, "Few-cycle optical waveform synthesis," Appl. Phys. B **72**, 373–376 (2001).

27. S. Rausch, T. Binhammer, A. Harth, F. Kärtner, and U. Morgner, "Few-cycle femtosecond field synthesizer," Opt. Express **16**, 17410–17419 (2008).

28. A. M. Weiner, "Femtosecond pulse shaping using spatial light modulators," Rev. Sci. Instr. **21**, 1929–1960 (2000).

29. M. Wollenhaupt, A. Assion, and T. Baumert, "Femtosecond laser pulses: Linear properties, manipulation, generation and measurement," in *Springer Handbook of Lasers and Optics,* , F. Träger, ed. (Springer, Berlin, 2007), pp. 937–983.

30. R. Trebino, K. DeLong, D. Fittinghoff, J. Sweetser, M. Krumbugel, B. Richman, and D. Kane, "Measuring ultrashort laser pulses in the time-frequency domain using frequency-resolved optical gating," Rev. Sci. Instr. **68**, 3277–3295 (1997).

31. B. E. Schmidt, W. Unrau, A. Mirabal, S. Li, M. Krenz, L. Wöste, and T. Siebert, "Poor man's source for sub 7 fs: a simple route to ultrashort laser pulses and their full characterization," Opt. Express **16**, 18910–18921 (2008).

32. B. E. Schmidt, O. Gause, F. Hagemann, S. Li, W. Unrau, L. Wöste, and T. Siebert, "Optimal white light control of the negative to neutral to positive charge transition (nenepo) in the electronic manifold of the silver trimer," J. Phys. Chem. A **116**, 11459–11466 (2012).

33. S. Weber, A. Lindinger, M. Plewicki, C. Lupulescu, F. Vetter, and L. Woste, "Temporal and spectral optimization course analysis of coherent control experiments," Chem. Phys. **306**, 287–293 (2004).

34. J. Vaughan, T. Feurer, K. Stone, and K. Nelson, "Analysis of replica pulses in femtosecond pulse shaping with pixelated devices," Opt. Express **14**, 1314–1328 (2006).

35. T. Brixner and G. Gerber, "Quantum control of gas-phase and liquid-phase femtochemistry," Chem. Phys. Chem. **4**, 418–438 (2003).

36. V. Lozovoy and M. Dantus, "Coherent control in femtochemistry," Chem. Phys. Chem. **6**, 1970–2000 (2005).

37. O. Kühn and L. Wöste, eds., *Analysis and Control of Ultrafast Photoinduced Reactions*, Springer Series in Chemical Physics, vol. 87, (Springer, Berlin 2007).

38. Y. Silberberg, "Quantum Coherent Control for Nonlinear Spectroscopy and Microscopy," Annu. Rev. Phys. Chem. **60**, 277–292 (2009).

1. Introduction

Recent developments for the generation and manipulation of high bandwidth ultrashort laser pulses are continuously improving the light sources available in the few to single cycle regime [1, 2]. Central to these efforts are strategies that provide extended nonlinear propagation under controlled conditions such as hollow core and photonic crystal fibers as well as filamentation [3–9]. In this context, self-compression to the single-cycle regime via filamentation in pressure gradients has been achieved and a low phase jitter in the preservation of the carrier envelope phase (CEP) during spectral broadening in filamentation has been demonstrated [10–12]. The self-compression to the few-cycle regime in two color, two-pulse co-filamentation further exemplifies the capabilities of cross-modulation strategies [13–15]. Efforts towards spectral broadening beyond the NIR and visible regime to include ultraviolet components are expanding this pulse compression technique into a spectral regime of short phase cycles [13, 16, 17]. In combination with these techniques, active optical elements such as liquid crystal arrays and microelectromechanical devices (MEMS) in pulse shaper arrangements have enabled the phase control necessary for effective pulse compression [17–24]. Phase correction with these types of systems can facilitate significantly enhanced pulse compression and a new regime of phase resolution has been demonstrated in liquid crystal double arrays when used as a common path interferometer for the generation of double pulse sequences [25]. Parallel to the developments for supercontinuum generation, optical waveform generation in the few-cycle regime with CEP stabilized laser pulses has been approached, utilizing broadband oscillators or spectral broadening in standard single mode fibers [26, 27]. In the following, a configuration is presented that seeks to contribute to these efforts by utilizing the precise phase manipulation of coherent supercontinuum pulses within a 4-f spatial light modulator arrangement for pulse form synthesis in the few-cycle regime.

2. Methodology

2.1. Experimental setup

As shown in Fig. 1, the general strategy for high-bandwidth pulse form synthesis is realized by sequential filamentation of amplified femtosecond laser pulses in air with an accompanying chirped mirror pre-compression and a subsequent spectral phase manipulation in a pulse shaper arrangement. The initial laser pulses are obtained from a standard femtosecond oscillator and amplifier system. A frequency-doubled Nd:Vanadate laser (Verdi V5, Coherent) pumps a Ti:Sapphire oscillator (Femtosource Compact, Femtolasers) giving laser pulses of 6 nJ centered at 805 nm with approximately 90 nm bandwidth at a repetition rate of 80 MHz. Standard Ti:Sapphire chirped pulse amplification (Odin C, Quantronix) is achieved in a multi-pass arrangement at 1 kHz by pumping with a nanosecond frequency-doubled Nd:YLF giving amplified pulses at 807 nm and a bandwidth of 46 nm with an adjustable pulse energy between 0.4 and 1.4 mJ and pulse durations of sub 40 fs.

For a mild spectral broadening of the initial output of the amplifier system, a first filamentation in air with a moderate pulse energy of 430 μJ is realized by focusing with a spherical mirror (SM1: R = 4000 mm) for initiating filamentation. Collimation and compression after filamentation is achieved with a spherical mirror (SM2: R = 5000 mm) and 2 double bounces on a GVD-oscillation compensated chirped mirror pair (CM1 and CM2: Layertec) with an average GVD of -60 fs^2/rad per double bounce over the spectral range of 700 to 900 nm. The pulses are attenuated to 300 μJ by means of an iris (I2) and guided into a second filamentation stage to extend the spectrum further into the visible spectral range. This is achieved by focusing and collimating with spherical mirrors (SM3 and SM4: R = 3000 mm and R = 2500 mm, respectively). Pre-compression of the generated supercontinuum is carried out after the second

filamentation stage with 10 double bounces on a second chirped mirror pair (CM3 and CM4: Layertec) with an average GVD of -40 fs^2/rad over the spectral range of 510 to 920 nm. The number of reflections for pre-compression after the second filamentation stage is chosen in view of the dispersion in the LC-SLM and optical path that follows. It is also important to note that the chirped mirror pair does not have a constant GVD over the full spectral range, which will be discussed in detail in the following section.
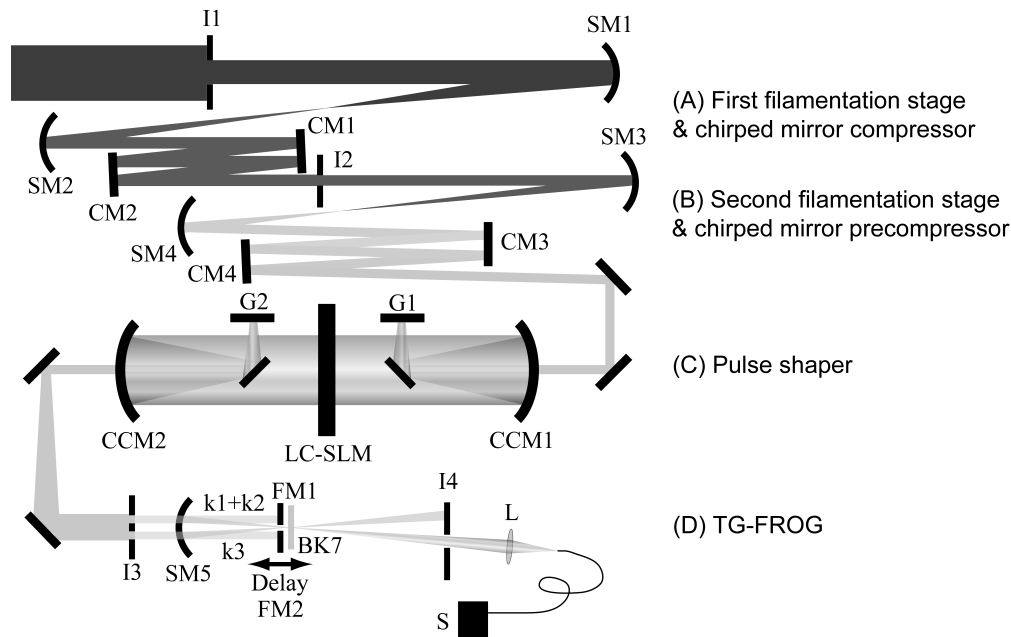

Fig. 1. Schematic of the experimental setup for supercontinuum generation and pulse shaping. (A) First filamentation stage and compression: (I1) iris, (SM1) concave spherical mirror, R = 4000 mm; (SM2) concave spherical mirror, R = 5000 mm; (CM1, CM2) chirped mirror pair, GVD -60 fs^{2}rad^{-1}/double bounce. (B) Second filamentation stage and pre-compression: (I2) iris; (SM3) concave spherical mirror, R = 3000 mm; (SM4) concave spherical mirror, R = 2500 mm; (CM3, CM4) chirped mirror pair, GVD -40 fs^{2}rad^{-1}/double bounce. (C) Pulse shaper: (G1, G2) diffraction grating, 300 l/mm and 600 nm blaze; (CCM1, CCM2) concave cylindrical mirrors, R = 500 mm; (LC-SLM) spatial light modulator, 2x640 pixels. (D) Frequency-resolved optical gating, TG-FROG: (I3) spatial filter; (FM1, FM2) D-shaped mirrors; (SM5) concave spherical mirror, R = 500 mm; (BK7) glass platelet, BK7; (I4) iris; (L) lens, f = 100 mm; (S) fiber spectrometer.

2.2. LC-SLM calibration

The spectrally broadened and pre-compressed supercontinuum pulses that range from approximately 550 to 900 nm at 10% maximum intensity are guided into a 4-f zero dispersion compressor setup (G1 and G2: silver reflection grating, 300 l/mm, 600 nm blaze, HORIBA - Jobin Yvon; CCM1 and CCM2, concave cylindrical mirrors, R = 500 mm) with a 640 pixel double array LC-SLM placed in the Fourier plane (SLM-640-D-VN, Cambridge Research & Instrumentation). The relative phase retardation attainable by transmission of the spectrally dispersed supercontinuum through the pulse shaper arrangement is strongly wavelength dependent, which necessitates an individual calibration of each pixel pair in the LC-SLM rather than a global calibration of the double array. This is accomplished by recording the transmission through an

analyzer (wire-grid polarizer, Edmund Optics) with a spectrometer (USB 2000, Ocean Optics) as a function of the voltage applied to the pixels of one array of the LC-SLM, while the voltage applied to the other array is held constant. The fast (x) and slow (y) axes of the liquid crystals in one array are orientated at 45 and -45° relative to the polarization of the input laser pulses with a 90° relative orientation of the crystals in the two pixel arrays. The transmission through the analyzer is described by the relation,

$$T_\omega(V) = \sin^2 \left(\frac{\varphi_y(V) - \varphi_x(V)}{2} \right) \tag{1}$$

with the voltage dependent transmission $T_\omega(V)$ at a specific spectral position ω and the corresponding phase retardations $\varphi_x(V)$ and $\varphi_y(V)$ for the fast and slow axis of the individual pixels [28]. A full oscillation of the transmitted signal as a function of voltage, *e.g.* from maximum to maximum, gives a π rotation of the polarization and a corresponding phase-retardation of 2π at a specific spectral position. The transmission measurement is shown in Panel C of Fig. 2 for three different pixels of the LC-SLM. In order to assign the phase retardation of a
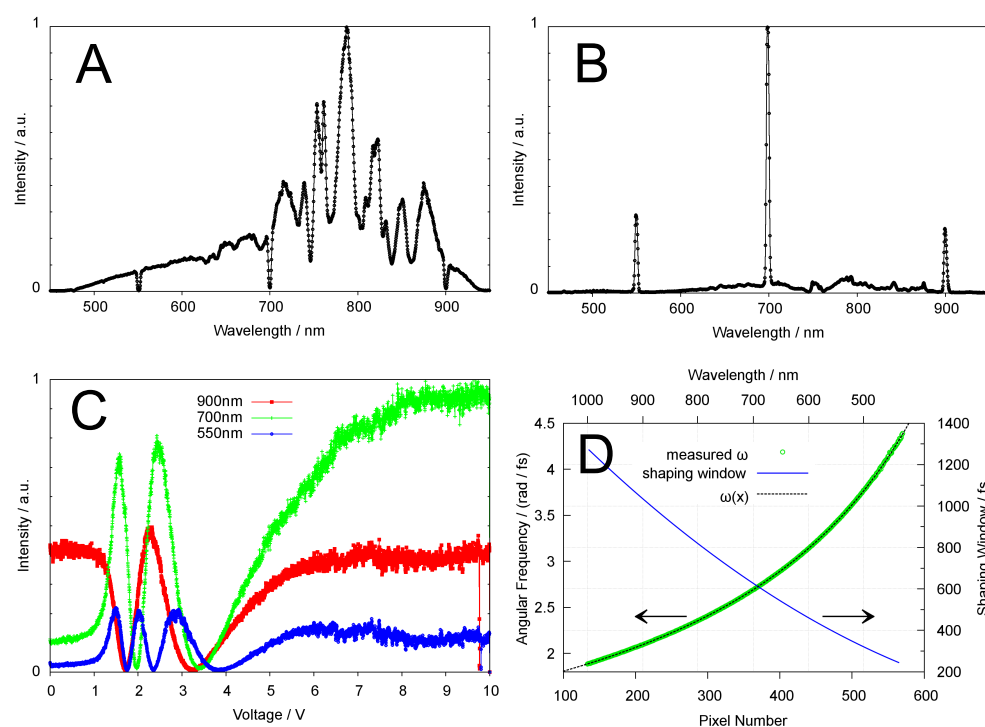

Fig. 2. (A) Supercontinuum spectrum after the SLM and polarization analysis set for full transmission except for a minimum transmission of three selected spectral channels at 550, 700 and 900 nm. (B) Complementary suppression of the full supercontinuum spectrum and full transmission through three selected pixels each at 550, 700 and 900 nm. (C) Calibration of the phase retardation giving the transmission for the spectral channels at 550, 700 and 900 nm after polarization analysis as a function of the voltage applied to one array of the LC-SLM. (D) Spectral calibration of the LC-SLM (green), fit function $\omega(x) = a/(x - x_0)$ (black dashed line) and the shaping window $\tau(x) = \pi/\omega'(x)$ (blue line) of the 4f pulse shaper arrangement. For details, see text.

specific spectral channel to a pixel, the spectral calibration of the pulse shaper is performed by scanning the phase retardation in one pixel while maintaining all other pixels constant and recording the transmitted spectrum of the selected pixel with the spectrometer. This procedure is scanned across all the pixels of the LC-SLM. Fitting each spectrum with a gaussian function yields the wavelength transmitted through the corresponding pixel. After spectral calibration, a phase retardation can be referenced to each pixel.

In order to provide an overview of the working parameters of the pulse shaper arrangement used in this work, the retardation measurement is shown for three exemplary spectral channels in Panel C of Fig. 2. The maximal phase amplitude attainable is shown to range from a little over 6π at 550 nm, approximately 5π at 700 nm to nearly 4π at 900 nm. The approximate bandwidth transmitted through three pixels at a particular spectral position is illustrated by setting the phase retardation to minimal transmission at 550, 700 and 900 nm after polarization analysis in Panel A of Fig. 2. Conversely, in Panel B of the same figure the same pixels are set to maximal transmission while suppressing the rest of the spectrum. The corresponding spectral resolution of the pulse shaper setup determines the shaping window τ, the maximal temporal shift achievable within the sampling limit $|\delta\phi| \leq \pi$, where $\delta\phi$ denotes the phase difference between two adjacent pixels. The shaping window is given by $\tau < \pi/\delta\omega$ with the bandwidth transmitted through a single pixel given by $\delta\omega$ [23, 28, 29]. In Panel D of Fig. 2, the spectral calibration data and the shaping window as a function of the wavelength or the pixel number is shown. The later is obtained by fitting the spectral calibration data (angular frequency ω versus pixel number x) with an analytical function $\omega(x) = a/(x - x_0)$ and calculating the shaping window $\tau(x) = \pi/\omega'(x)$. Hereby, $\omega(x) = a/(x - x_0)$ with the parameters a and x_0 is a small-angle approximation for the projection of the spectrum onto the LC-SLM. The shaping window ranges from more than a picosecond above 900 nm to a mere 300 fs at 500 nm.

2.3. Pulse characterization (FROG)

The characterization of the initial amplified pulses, the intermediate pulses from filamentation and the final pulse forms generated with the pulse shaper is achieved via frequency-resolved optical gating (FROG) in a transient grating (TG), four-wave mixing geometry [30]. The arrangement has been described in previous work [31, 32]. Briefly, the laser pulses are guided through a spatial filter (I3) that separates the beam into three equivalent sub-pulses (k_1, k_2, and k_3). A split mirror arrangement (FM1 and FM2) allows for a relative temporal delay of one of the three sub-pulses (k_3) via a mechanical stage (PLS-85, MICOS) and all three pulses are focused at equal angles in a folded-boxcars arrangement with a common spherical mirror (SM5, R = 500 mm) into a 0.17 mm thick BK7 glass platelet (BK7). The coherent four-wave mixing signal is obtained in the direction $k_s = k_1 - k_2 + k_3$ from scattering the delayed sub-pulse (k_3) on the transient optical grating induced by the other two sub-pulses (k_1 and k_2) in the platelet. This signal is spatially filtered from the other three beams with an iris (I4) and detected with a spectrometer (USB2000, Ocean Optics) as a function of the temporal delay of k_3 relative to the pulse pair, k_1 and k_2. Hereby, the phase matching is determined by the nature of the phase grating. Particularly the path length of the coherence volume generated by the superposition of the pulse pair k_1 and k_2 in the glass platelet determines the bandwidth for phase-matched scattering of k_3. This allows for the flexibility to correlate pulses ranging over variable time scales and bandwidth.

3. Results and discussion

3.1. Spectral broadening and pulse compression

In order to provide maximal bandwidth for pulse compression and pulse form synthesis, the route to enhanced spectral broadening via a two-stage filamentation originally established by

Keller and coworkers is applied here at moderate pulse energies and corresponding peak powers [10, 31]. This is one possible route for attaining significant contributions in the visible region of the supercontinuum while simultaneously avoiding a complex spectral phase in the NIR spectral region when high bandwidth pulses are generated at elevated intensities [6, 10]. The sequence of FROG traces in Fig. 3 and 4 illustrates the pathway of spectral broadening and pulse compression from the initial amplifier output to the final supercontinuum pulses after two-stage filamentation with chirped mirror pre-compression and a refined post-compression in the pulse shaper. In Panel A and B of Fig. 3, the FROG trace and spectrum of the initial pulse from the femtosecond amplifier is shown. The seed pulse for filamentation shows no relevant second order phase contributions and has a duration of 35 fs with a bandwidth of 46 nm FWHM. Deviations of the pulse duration from the transform limit for this bandwidth are attributed to residual third order phase contributions. The pulse was attenuated to 430 μJ, which corresponds to filamentation at a peak power of 12 GW.

While single-stage filamentation with input pulses above the microjoule domain at peak powers > 20 GW and intensities > 5.0×10^{13} W/cm^2 shows advantageous stability and spectral broadening with a positive pre-chirp [10, 31], filamentation at moderate conditions was best realized at pulse compression with maximal GVD compensation, which leaves a residual TOD component on the amplified pulse as shown in Panel A of Fig. 3. Under these conditions, filamentation in air leads to a structured spectrum shown in Panel D of Fig. 3 that ranges roughly from 760 to 860 nm, giving a bandwidth of approximately 80 nm at FWHM. A FROG trace taken after 2 double bounces in the chirped mirror compressor is shown in Panel C of Fig. 3.
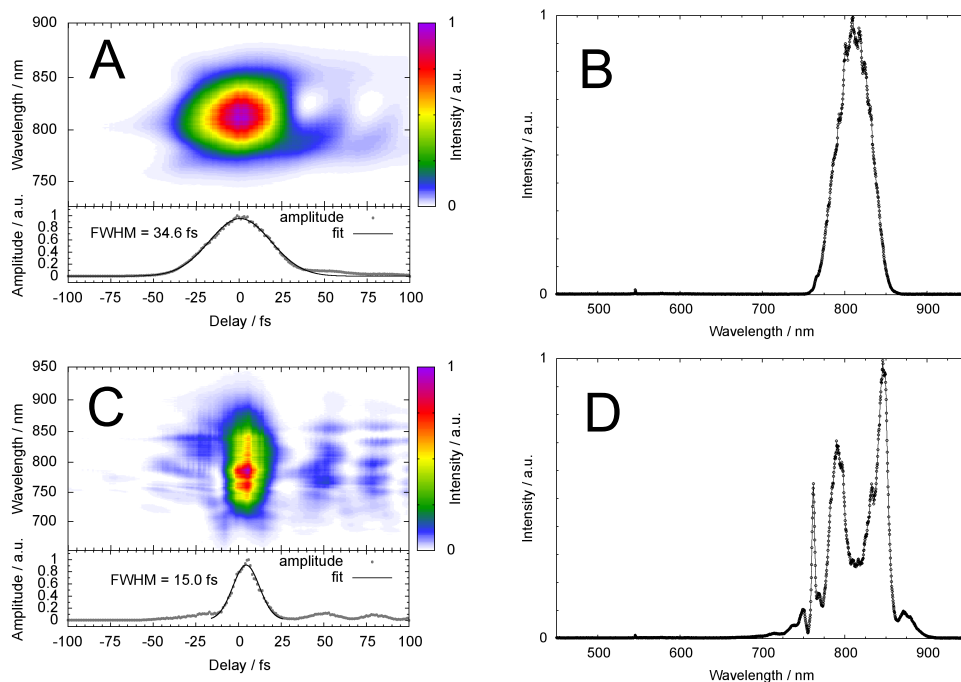

Fig. 3. Sequence of spectral broadening and pulse compression in the experimental setup shown in Fig. 1. (A) FROG trace and (B) spectrum of the input pulse from the femtosecond amplifier. (C) FROG trace and (D) spectrum after first filamentation stage and chirped mirror pulse compression.

With a total GVD correction of -120 fs^2/rad, a compression to 15 fs can be attained in the first filamentation stage with a final pulse energy of 400 μJ. The high transmission of approximately 90% together with the significant compression is essential to attain sufficient nonlinearity for spectral broadening in the second filamentation stage. After spatial filtering with an iris, the resulting attenuation to 300 μJ provides a peak power of approximately 20 GW for further filamentation.

The supercontinuum obtained from filamentation with these pulse parameters is shown in Panel B of Fig. 4. Panel A shows the FROG trace of the pulse after the chirped mirror pre-compression with the pulse shaper set to zero phase. Panel C and D give the respective FROG trace and spectrum after full pulse compression with the spectral phase applied to the pulse shaper that is given in Panel D (blue squares). A significant spectral broadening to a bandwidth of approximately 350 nm at 10% maximum over the visible to NIR range from 550 - 900 nm is documented after the chirped mirror pre-compression and spatial light modulator post-compression. In comparison to single-stage filamentation, the contrast in the spectral power density between the visible to NIR spectral contributions is significantly reduced. This enhanced yield of visible contributions in the supercontinuum spectrum is critical for efficient pulse compression and further utilizing the full bandwidth for pulse form synthesis in the pulse shaper. The final pulse energy obtained after the pulse shaper is 60 μJ, which translates to a
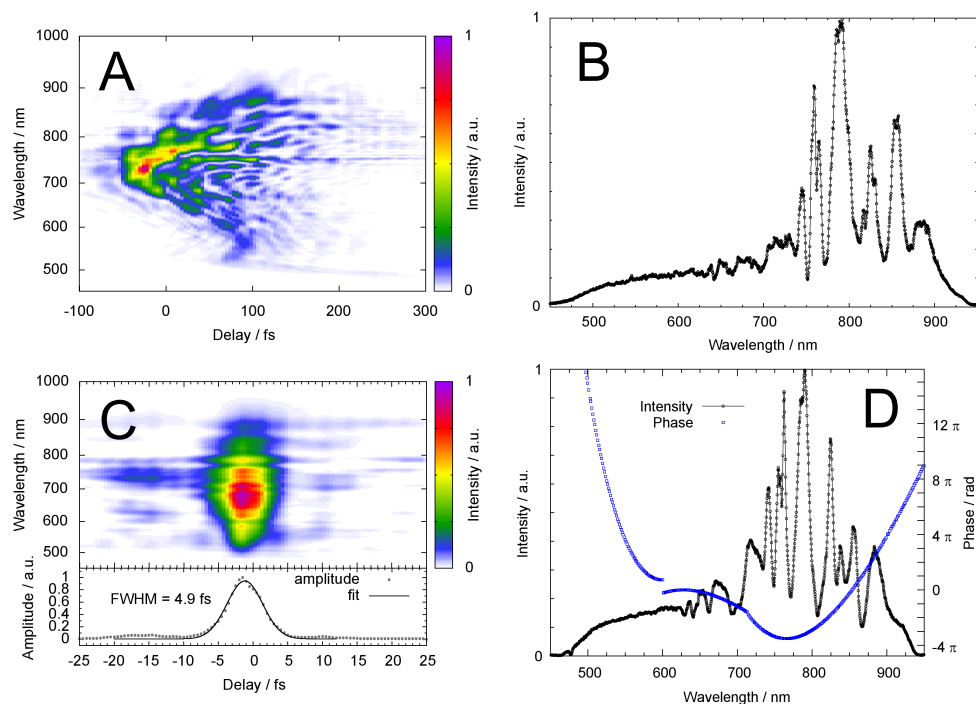

Fig. 4. Sequence of spectral broadening and pulse compression in the experimental setup shown in Fig. 1. (A) FROG trace after chirped mirror pre-compression (10 double bounces, -400 fs^2/rad) and pulse shaper set to zero phase. (B) Spectrum after the second filamentation stage. (C) FROG trace and (D) spectrum (black points) after compression with the spectral phase composed of three second-order phase functions shifted temporally against one another with additional linear phase ramps (blue squares) set on the pulse shaper (for details see Table 1).

transmission of 20% for this second compression stage and a total transmission of 14% with respect to the initial input pulse. The primary energy losses for this compression stage can be attributed to the gratings of the pulse shaper arrangement. The typical pulse duration of 4.9 ± 0.4 fs shown in the FROG trace of Panel C in Fig. 4 is achieved with 10 double bounces in the second chirped mirror compressor resulting in a total GVD correction of -400 fs^2/rad together with a refined phase correction in the pulse shaper.

As shown in Panel D of Fig. 4, the total phase function applied to the LC-SLM to achieve the final compression is divided into three spectral regions of second-order phase corrections. These are temporally shifted with an additional linear phase ramp, vary in amplitude and alternate from negative to positive. The functions are explicitly given in Table 1 according to the formalism summarized by Wollenhaupt *et. al* [29]. While the pulse shaper allows for more complex phase corrections to be realized by including contributions of higher order phase functions, this simple and analytical correction allows for stable and reproducible compression to pulse durations below 5 fs. To understand the strategy of dividing the phase function for compression into this discrete set of second-order corrections in different spectral regions, it is important to consider the pre-compression with the respective chirped mirror pair that follows the second filamentation. While the average GVD from 510 to 920 nm is given at -40 fs^2/rad per double bounce, this value is not constant for all wavelengths. When 10 double bounces are utilized for

Table 1. Summary of the transfer function of the LC-SLM used for pulse compression and shaping of the supercontinuum following the formalism summarized by Wollenhaupt *et. al.* in the Taylor expansion of the complex spectral phase function with the respective coefficients [29]. Unless specified, $\omega_0 = 3.0$ rad/fs and for 7(B) the equivalent quadratic phase function is given that is adjusted to the sampling points. For details see text.

Fig.	Spectral Range	Phase Function, $\varphi(\omega)$	Coefficients, b_n
4.(D)	500-600 nm	$b_1(\omega - \omega_0)^2 + b_2\omega$	$b_1 = +113$ fs^2/rad $b_2 = -32$ fs
	600-714 nm	$b_1(\omega - \omega_0)^2$	$b_1 = -39$ fs
	714-950 nm	$b_1(\omega - \omega_0)^2 + b_2\omega$	$b_1 = +173$ fs^2/rad $b_2 = +187$ fs
5.(A)	500-950 nm	$b_1 \sin(b_2\omega + b_3)$	$b_1 = +2.0$ rad $b_2 = +20$ fs $b_3 = +4.0$ rad
5.(B)	500-950 nm	$b_1 \sin(b_2\omega + b_3)$	$b_1 = +2.2$ rad $b_2 = +50$ fs $b_3 = 0.0$ rad
6.(A)	500-724 nm	0	–
	724-950 nm	$b_1\omega$	$b_1 = -600$ fs
6.(B)	500-724 nm	0	–
	724-950 nm	$b_1\omega$	$b_1 = +600$ fs
6.(C,D)	500-700 nm	$b_1\omega$	$b_1 = -400$ fs
	700-950 nm	0	–
7.(B)		$b_1(\omega - 3.05 \text{ rad/fs})^2 + b_2\omega + b_3$	$b_1 = -550$ fs^2/rad $b_2 = +585$ fs $b_3 = +4.25$ rad

a best possible compromise in pre-compression over the full supercontinuum spectrum, a substantial residual phase is accumulated from the chirped mirror pair. This is evident in the FROG trace of the pre-compressed pulse with a zero phase written on the LC-SLM, shown in Panel A of Fig. 4. The FROG trace clearly shows a negative linear chirp in the spectral region above 700 nm, a positive linear chirp from 700 nm to approximately 600 nm and a negative chirp from 600 nm to 510 nm. By utilizing this FROG trace, the phase function for compression could be approximated. The refined phase function for best possible compression is given in Table 1.

3.2. Supercontinuum pulse shaping

3.2.1. Pulse train generation

Beyond the possibility of a refined pulse compression outlined above, the pulse shaper provides the capability to generate different pulse forms at supercontinuum bandwidths [20, 32]. For demonstrating this capability, particular emphasis is made on the temporal resolution and contrast that can be retained when the function of the spatial light modulator is expanded to the writing of analytical phase functions on the supercontinuum spectrum. Two examples are chosen in order to illustrate different aspects of pulse form synthesis in the few cycle regime. In the generation of pulse trains as shown in Fig. 5, the corresponding phase function extends
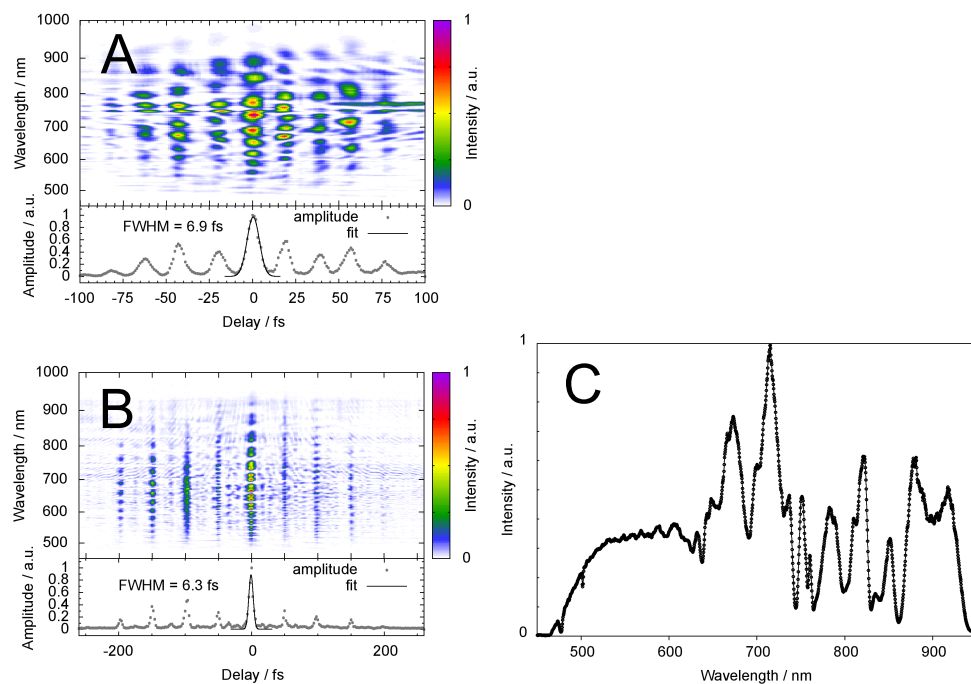

Fig. 5. (A) and (B): FROG traces of supercontinuum pulse trains with a sub-pulse spacing of 20 and 50 fs, utilizing a sinusoidal phase function with a modulation frequency of $\Delta T^{-1} = 50$ and 20 THz at a modulation depth of 2.0 and 2.2 rad, respectively. The explicit phase functions are given in Table 1. (C) Spectrum of the 50 fs pulse train measured after the pulse shaper, where a dichroic beamsplitter (R = 80% from 750 to 850 nm) attenuates the NIR spectral region for equal contributions of the visible and NIR components to the supercontinuum spectrum.

continuously over the full spectral envelope, resulting in a pulse form that utilizes the full bandwidth over its entire duration. The limitations imposed by discrete sampling of this phase function via the LC-SLM is determined by the frequency and amplitude of the periodic modulation. Alternatively, the generation of double pulse structures as given in Fig. 6 demonstrates the application of a discontinuous phase function for a defined temporal sequencing of selected spectral components. For this case, only the slope of the phase used for temporal delay of a specific spectral region of the supercontinuum is relevant with respect to the sampling limit of the LC-SLM. Since the phase function used for pulse compression is the starting point for both pulse forms, the slope of the total phase function composed of the contribution necessary for pulse compression and the contribution for pulse shaping must be considered.

For the case of pulse train generation, Panel A and B of Fig. 5 show the FROG traces of the pulse shapes attained via phase-only modulation with a sinusoidal function superimposed on the spectral phase for pulse compression. A spectral modulation period ΔT^{-1} of 50 and 20 THz corresponds to a temporal separation of the sub pulses ΔT of 20 and 50 fs at a modulation depth of 2.0 and 2.2 rad, respectively. Notably, the sub-pulse duration for both cases is maintained in the sub 7 fs regime. The starting point for generating the 50 fs pulse train was a short pulse compressed with a phase similar to that shown in Panel D of Fig 4. Furthermore, the supercontinuum spectrum utilized for the generation of the 50 fs pulse train, shown Panel C of Fig. 5, was modified with a dichroic beamsplitter (Layertec, R=80% at 750 and 850 nm) to achieve nearly equal amplitude in the NIR and VIS components. Due to the dispersion introduced by the beamsplitter, the phase function for compression was modified accordingly. The starting point for the 20 fs pulse train was a compressed pulse obtained with a genetic algorithm by optimizing the intensity of the FROG signal at zero delay rather than an analytical phase function as shown in Panel D of Fig. 4 [32, 33]. Further refining the pulse compression with a genetic algorithm allowed for cleaner pulse trains with a higher contrast at shorter sub-pulse delays.

3.2.2. Double pulse structures

In order to further illustrate the capabilities and limitations of pulse forming at supercontinuum bandwidths, the FROG traces in Panel A to C of Fig. 6 show double pulse structures that split the spectrum into two discrete regions with variable temporal delay between the selected spectral components. The starting point for the generation of these double pulse sequences was a short pulse compressed with a phase similar to the function shown in Panel D of Fig. 4. In Panel A and B of Fig. 6, the NIR part of the spectrum above 724 nm was shifted by -600 fs and 600 fs, respectively, using a linear phase ramp with an equivalent slope of ± 600 fs applied to this part of the spectrum. The rest of the spectrum was maintained at zero phase relative to the phase function of the compressed pulse form. The explicit functions employed for generating these double pulse structures are also given in Table 1. Due to the higher spectral resolution of the pulse shaper in the NIR spectral range, temporal shifting in this spectral region is more advantageous in comparison to actively shifting the visible region of the spectrum as documented in the calibration of the LC-SLM summarized in Fig. 2.

In order to demonstrate the limitations imposed by discrete phase sampling for a temporal delay close to the shaping window, a FROG trace of a double pulse sequence is shown in Panel C of Fig. 6, where the visible part of the spectrum below 700 nm was shifted by -400 fs with the respective phase ramp and the NIR region above 700 nm is maintained at zero phase. The visible sub-pulse suffers from substantial loss in intensity and a chirped replica pulse can clearly be seen in the region between +300 and +800 fs delay in the cropped version of the FROG trace shown in Panel D of Fig. 6. Since the spectral resolution of the pulse shaper decreases with the wavelength, the replica pulse has a strong negative chirp. To understand the origin of the replica pulse, the spectral phase function applied to the LC-SLM is depicted in Panel

A of Fig. 7, consisting of the phase for initial pulse compression and the linear phase ramp for temporal shifting. The formation of the replica pulse for this case can be illustrated by the phase function shown in its wrapped form around 3.05 rad/fs in Panel B of Fig. 7 together with the points sampled by the LC-SLM. Due to the dispersion in the spectral resolution over the LC-SLM, the sampled points of the linear function with a negative slope of -400 fs (black line, Panel B of Fig. 7) can be interpreted as second order phase function with varying positive slope (red line, Panel B of Fig. 7) [34]. The parameters for this second order phase function can be extracted directly from the replica pulse in the FROG trace, which shows a temporal shift of about +600 fs at 3.05 rad/fs (≈ 617 nm), a shift of 700 fs at 2.89 rad/fs (≈ 650 nm) and a shift of 550 fs at 3.13 rad/fs (≈ 600 nm). From these points, a spectral phase function according to $\phi(\omega) = b_2(\omega - \omega_0)^2 + b_1(\omega - \omega_0)$ can be formulated with a $b_2 = -625$ fs^2/rad, $b_1 = 600$ fs and $\omega_0 = 3.05$ rad/fs. The parameters were adjusted slightly to match the points sampled by the LC-SLM. Both functions equivalently represent the spectral phase written by the LC-SLM and the correspondence to the resulting replica pulse illustrates the effects that occurr when operating at the limit of the shaping window of the pulse shaper. The original linear phase ramp as well as the equivalent quadratic phase function depicted in Panel B of Fig. 7 are given in Table 1.
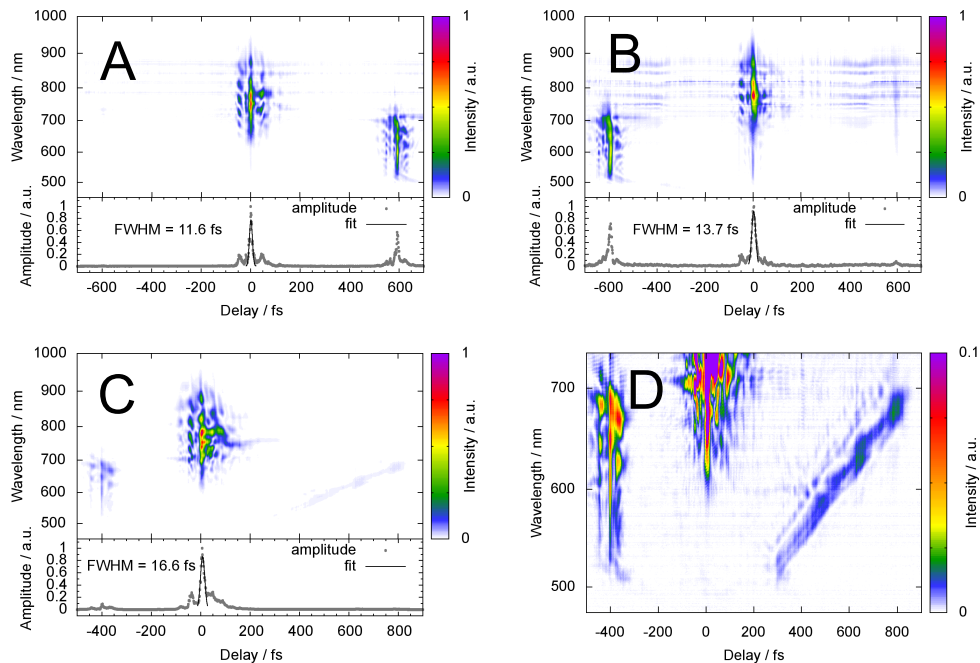

Fig. 6. (A) and (B): FROG traces of double pulses split at 724 nm (2.60 rad/fs) with a sub-pulse spacing of 600 fs. The IR part of the spectrum was temporally shifted by a linear phase ramp with a slope of ± 600 fs, respectively, in the spectral region above 724 nm. The rest of the spectrum was maintained at zero phase relative to the phase function employed for pulse compression. (C) and (D): FROG trace of a double pulse split at 700 nm (2.69 rad/fs) with a sub-pulse spacing of 400 fs. The spectrum below 700 nm was temporally shifted using a linear phase ramp with a slope of -400 fs. The explicit phase functions are given in Table 1.
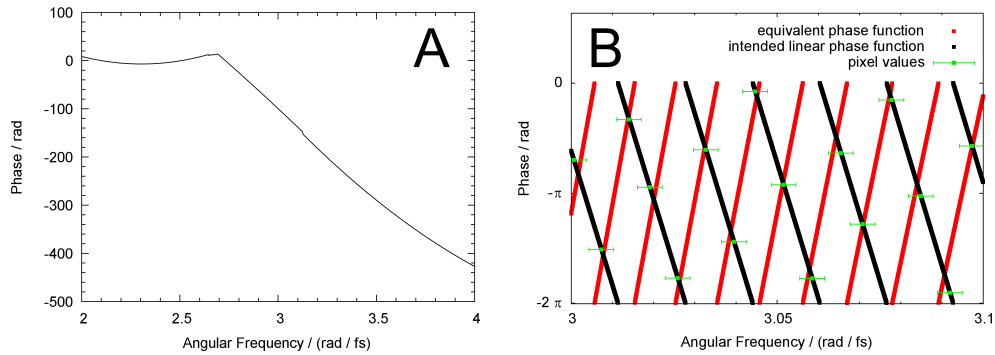
Fig. 7. (A) Total phase function for the pulse form shown in Panel C of Fig. 6 resulting from the phase correction employed for pulse compression similar to Panel D of Fig. 4 and a linear phase ramp with a slope of −400 fs above 2.69 rad/fs (700 nm). (B) Magnification of the phase function in the region around 3.05 rad/fs in a wrapped representation (black line). Points sampled by the LC-SLM (green points) with error bars indicating the approximate bandwidth transmitted through the corresponding pixels. An equivalent quadratic function (red line) is derived from the parameters of the sampling artifact for representing the linear phase ramp within the sampling limit of the LC-SLM. The original linear phase ramp and equivalent (within the sampling limit of the pulse shaper) quadratic phase function are summarized in Table 1. For details, see text.

4. Conclusion

The general capabilities and limitations of pulse form synthesis in the few-cycle regime at supercontinuum bandwidths with phase-only modulation have been demonstrated. The spectral broadening via double stage filamentation plays a critical role in supplying significant contributions of the visible region to the supercontinuum. This is essential for utilizing the corresponding frequencies in this spectral range for efficient pulse compression and flexible pulse shaping. Within this configuration for spectral broadening, pulse compression of the full supercontinuum to sub 5 fs can be easily achieved with a spatial light modulator that allows for a flexible adaptation to the spectral phase obtained from filamentation and chirped mirror precompression. The degree of pulse compression defines the temporal resolution and contrast attainable in pulse form synthesis. Two types of analytical pulse shapes are chosen in order to illustrate the time resolution, contrast and the sampling limit of the pulse shaper. Specifically, a continuous periodic phase modulation over the full bandwidth of the supercontinuum is employed for generating pulse trains. Double pulse structures are demonstrated with a discontinuous linear spectral phase that separates the spectral components of the supercontinuum into definable temporal events. For both cases, few-cycle sub-pulse durations are maintained in pulse forms that extend into the regime of hundreds of femtoseconds in total duration.

The potential of a light source that provides spectral channels from the visible to near infrared with variable temporal sequencing and high time resolution at pulse energies in the midmicrojoule domain has been demonstrated with selected examples. This is complemented by a transient grating FROG techique for a highly versatile pulse form analysis at supercontinuum bandwidths that allows for the correlation of pulse forms extending over several hundred femoseconds composed of ultrashort sub-pulse events. Within the general efforts towards expanding ultrashort light sources in their spectral range, bandwidth and pulse compression capabilities, a variety of nonlinear propagation strategies have been realized in different constellations and media with self-compression or active phase correction down to the single-cycle

regime in carrier envelop phase (CEP) stabilized scenarios as well as spectral broadening beyond the single-octave range [1, 3, 4, 9, 11, 13, 14, 16, 18, 20–22]. Among these advancements, spectral broadening via double filamentation as demonstrated in this work offers supercontinuum bandwidths with an advantageous distribution in the power density over a wide spectral range for pulse compression and shaping within an uncomplicated experimental arrangement. In combination with an active LC-SLM phase manipulation, an adaptive pulse compression mechanism and a versatile technique for pulse form synthesis at supercontinuum bandwidths is realized that is highly suited for a broad range of applications in ultrafast spectroscopy and coherent control scenarios [35–38]. In view of further developments, the pulse compression and synthesis of particular pulse forms have been carried out within a phase-only modulation mode of the pulse shaper and an amplifier system that supplies input pulses with varying CEP. With respect to the former, expanding the operating mode of the pulse shaper to phase and amplitude modulation allows for a balanced contribution of all the spectral channels within the supercontinuum. This supplies more effective bandwidth for enhanced pulse compression as well as a higher flexibility in controlling specific spectral channels within a particular pulse form.